Hydraulic Bulge Test of Al and Copper Tubes

Dr. Azal Rifaat Ismail
Production and Metallurgy Engineering Department, University of Technology/ Baghdad
Email:Sami-abbasaa@yahoo.com
Sami Abbas Hammood
Production and Metallurgy Engineering Department, University of Technology/ Baghdad

Received on: 3/2/2013 & Accepted on: 9/5/2013

ABSTRACT

This work aims to find forming limit diagram and mechanical properties experimentally to measure formability by hydraulic bulge test and tensile test, and determination the values of the bursting pressure and final thickness in the final stage at bursting experimentally and numerically by using program (ANSYS 11) to perform numerical simulation for copper and aluminum alloy (6060) tubes before and after heat treatment by hydraulic bulge test.

In this work, used two types of tubes with dimensions for copper of (L_0=150mm, d_0 = 41.275mm, t_0 = 1.06mm) and for aluminum alloy (6060) are (L_0=150mm, d_0 = 60mm, t_0 = 2 mm). Applied heat treatment (annealing) of copper and aluminum tubes at temperature (450°C, 400°C).the holding time in the furnace was 1 hour and then cooled in the furnace. Has been printed square grid by screen method with dimensions (5x5 mm) for copper and aluminum tubes before and after heat treatment and with dimensions (2.5x2.5 mm) for tensile samples of copper and aluminum before and after heat treatment. Strain Measurement accomplished by using image processing technology using MATLAB by measuring the dimensions of the grid printed before and after the deformation and then measure the true strain on tensile samples and tubes used in the tensile test and hydraulic bulge test before and after heat treatment.

The results show that, the values of the bursting pressure and final thickness in the final stage at bursting for copper tube before and after treatment is (29MPa, 27MPa)،(0.892mm, 0.621 mm) and for aluminum tube before and after treatment is (19MPa, 16MPa),(1.789mm, ١,٤٨٧٢ mm). Increasing formability and decreasing bursting pressure of tubes after heat treatment of increasing the strain hardening exponent (n) of tubes.

تشكيل انابيب النحاس والالمنيوم باختيار ضغط الانفجار

الخلاصة

يهدف هذا البحث للحصول على مخطط حد التشكيل والخواص الميكانيكية عمليا لقياس قابليه التشكيل بواسطة اختبار الانتفاخ الهيدروليكي واختبار الشد، وحساب قيم كل من ضغط الانفجار والسمك النهائي في المرحلة النهائية في اختبار الانتفاخ عمليا وعدديا باستخدام برنامج

https://doi.org/10.30684/etj.31.15A.11
2412-0758/University of Technology-Iraq, Baghdad, Iraq

(ANSYS 11) لانجاز المحاكاة لانابيب من النحاس وسبيكة الألمنيوم (6060) قبل وبعد المعاملة الحرارية عن طريق اختبار الانتفاخ الهيدروليكي. في هذا العمل استخدم نوعين من أنابيب النحاس مع أبعاد هي (L_0 =150mm, d_0 = 41.275mm, t_0 = 1.06mm) وسبيكة الألومنيوم (6060)هي (L_0 =150mm, d_0 = 60mm, t_0 = 2 mm) . تم اجراء معاملة حرارية (تلدين) لانابيب النحاس وأنابيب الألمنيوم عند درجة حرارة(400°C, 450°C) وابقيت في الفرن لمدة ساعة واحدة ثم بردت في الفرن . تم طباعة شبكة مربعة بطريقة السكرين وبإبعاد (5x5 mm) لأنابيب النحاس والألمنيوم قبل وبعد المعاملة الحرارية وبإبعاد (2.5x2.5 mm) لعينات الشد للنحاس والألمنيوم قبل وبعد المعاملة الحرارية. قياس الانفعال تم انجازه باستخدام تقنية معالجة الصور باستخدام برنامج MATLAB من خلال قياس إبعاد الشبكة المطبوعة قبل وبعد التشويه ثم قياس الانفعال على عينات الشد والأنابيب المستخدمة في اختبار الشد واختبار الانتفاخ الهيدروليكي قبل وبعد المعاملة الحرارية.

فقد بينت النتائج أن قيمة ضغوط الانفجار والسمك النهائي عن الانفجار لأنابيب النحاس قبل وبعد المعاملة الحرارية هي (27MPa, 29MPa)،(0.621mm, 0.892mm) وللألمنيوم قبل وبعد المعاملة الحرارية هي(16MPa, 19MPa), (1.789mm, ١,٤٨72mm). زيادة قابليه التشكيل وانخفاض ضغط الانفجار للأنابيب بعد المعاملة الحرارية وذلك لزيادة اس التصليد الانفعالي للانابيب .

INTRODUCTION

During tube hydroforming, several forming parameters, including the loading path, material properties, die design, and friction at the tube–die interface, significantly influence the results. For example,Ahmed and Hashmi (1997) proposed a theoretical method to estimate the forming parameters required for hydraulic bulge forming of tubular components; in particular, they studied the factors of internal pressure, axial load and clamping load. Sokolowski et al. (2000) proposed a tooling and experimental apparatus to determine the material properties of tubes. Vollertsen and Plancak (2002) proposed a principle for the measurement of the coefficient of friction in the forming zone. Lei et al. (2002) used the rigid-plastic finite element method combined with a ductile fracture criterion to evaluate the forming limit of hydroforming processes. The present authors (Hwang and Lin, 2006) proposed a mathematical model considering the forming tube as an ellipsoidal surface for the pur pose of analyzing the forming pressure and maximum bulge height. The properties of tubular materials were additionally evaluated by hydraulic bulge tests combined with the above-proposed analytical model (Hwang and Lin, 2007).

The forming limit diagram (FLD) of tubular materials ought to be established, because it directly influences the formability of the hydraulic forming processes. A few studies concerning the loading paths or the forming limit of tubes and sheets have been reported. For example, Tirosh et al. (1996) explored an optimized loading path for maximizing the bulge strain between necking and buckling experimentally with aluminumA5052 tubes. Zhao et al. (1996) discussed analytically and experimentally the effects of the strain rate sensitivity of the sheet material on the FLD in sheet metal forming based on the M–K model and Graf–Hosford anisotropic yield function. They found that FLDs with different pre-strains are signif icantly influenced by the straining paths. However, the converted forming limit stress diagrams (FLSD) appear not to be strongly influenced by the straining paths. Xing and Makinouchi (2001) investigated the differences in forming limits of tubes under internal pressure, independent axial load or torque

based on Yamada's plastic instability criteria and Hill's quadratic yield function. The above theory coupled with an in-house finite element code ITAS3d was used to control the material flow and to prevent the final failure modes from occurring. Nefussi and Combescure (2002) used Swift's criteria for sheets and tubes and took into account the buckling inducedby axial loading inorder to predict plastic instability for tube hydroforming. They concluded that the two Swift's criteria are applicable to predict necking and that a special attention has to be paid to plastic buckling, because the critical strains corresponding to buckling are much smaller than the critical strains predicted by the necking criteria. However, experiments are required to validate their theoretical results. Yoshida and Kuwabara (2007) discussed the FLD of steel tubes subjected to a combined axial load and internal pressure. They proposed a FLSD, and concluded that the forming limit stress of the steel tube is not fully path-independent and that the path dependence of forming limit stress is strongly affected by the strain hardening behavior of the material for given loading paths. Korkolis and Kyriakides (2008) investigated the performance of Hosford and Karafillis-Boyce non-quadratic anisotropic yield functions in predicting the response and bursting of tubes loaded under combined internal pressure and axial load. They concluded that the predicted structural responses are generally, but not universally, in good agreement with the experimental results, while the predicted strains at the onset of rupture are somewhat larger than the values measured. So far, a consistent conclusion for forming limit theorems of tubular materials has not been established and the forming limit diagram for AA6011 tubes has not been found.

THEORETICAL CONSIDERATIONS

Consider a tube which is subjected to an internal pressure, *pi*, and compressive axial forces, *F*, Figure (2) For an element at the middle of this tube, the following equilibrium equations of pressure vessel as shown in Figure (1) can be written. [4]

$$\frac{\sigma_1}{\rho_1} + \frac{\sigma_2}{\rho_2} = \frac{p_i}{t_i} \qquad \text{... (1)}$$

And

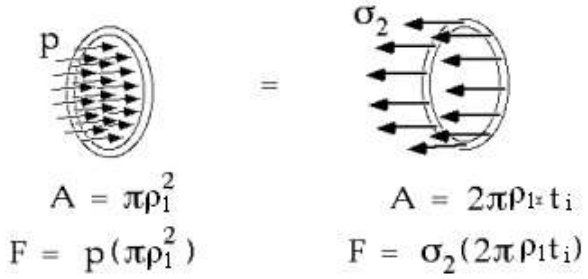

Figure (1) force calculation by equilibrium equations.

From Figure (1)

$F = p_i \pi \rho_1^2 - \sigma_2 (2 \pi \rho_1 t_i)$

$$\sigma_2 = \frac{p_i \rho_1}{2t_f} - \frac{F}{2\pi\rho_1 t_f} \quad \text{... (2)}$$

Effective stress and strain under Von Mises yield criterion and plane _stress condition are

$\sigma = 1/\sqrt{2}\ [(\sigma_1 - \sigma_2)^2 + (\sigma_2 - \sigma_3)^2 + (\sigma_3 - \sigma_1)^2]^{1/2}$

$$\bar{\sigma} = (1 - \alpha + \alpha^2)^{1/2} \cdot \sigma_1 \quad \text{... (3)}$$

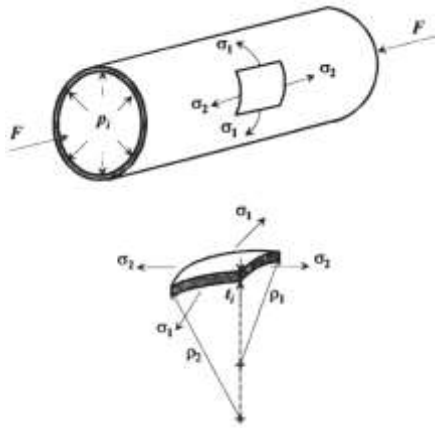

Figure (2) The stresses acting on an element at the *middle* of the tube.[4]

_and

$\epsilon = \sqrt{2}/3\ [(\epsilon_1 - \epsilon_2)^2 + (\epsilon_2 - \epsilon_3)^2 + (\epsilon_3 - \epsilon_1)^2]^{1/2}$

$\epsilon_1 + \epsilon_2 + \epsilon_3 = 0$, $\epsilon_3 = -(\epsilon_1 + \epsilon_2)$, $\epsilon_3 = -(\epsilon_1 + \beta\,\epsilon_1)$

$\epsilon_3 = -\epsilon_1 (1+\beta)$, $\epsilon_2 = \epsilon_1 \beta$ where (β- is strain ratio)

$$\bar{\epsilon} = \left[\frac{4}{3}(1 + \beta + \beta^2)\right]^{1/2} \cdot \epsilon_1 \quad \text{... (4)}$$

where

and $\alpha = \sigma_2/\sigma_1$ **... (5)**

$\beta = \epsilon_2/\epsilon_1$ **... (6)**

The tangential and radial strains, ϵ_1 and ϵ_3, can be denoted as

$$\epsilon_1 = \ln(\rho_1/\rho_0) \quad \text{... (7)}$$

and

$$\epsilon_3 = \ln(t_i/t_0) \quad \text{... (8)}$$

where ρ_0, ρ_1 are the initial and instantaneous radius of tube receptively , and t_0 t_i, are the initial and instantaneous tube wall thickness. Levy–Mises flow rule yields (assuming volume constancy)

$$\alpha = (2\beta + 1)/(2 + \beta) \quad \text{... (9)}$$

or

$$\beta = (2\alpha - 1)/(2 - \alpha) \quad \text{... (10)}$$

Combining Eqs. (2-1)–(2-3) and(2-5), one can write

$$p_i = \frac{\bar{\sigma}}{(1 - \alpha + \alpha^2)^{1/2}} \cdot t_i \cdot \left(\frac{1}{\rho_1} + \frac{\alpha}{\rho_2}\right) \quad \text{... (11)}$$

And

$$F = p_i \cdot \pi \cdot \rho_1^2 \cdot \left(1 - \frac{2\alpha}{1 + \alpha \cdot \rho_1/\rho_2}\right) \quad \text{... (12)}$$

At the interface between partial plastic deformations, one can write or assume that

$$\rho_1 = (d_0 - t_0)/2 \quad \text{... (13)}$$

$$\rho_2 = \infty \quad \text{... (14)}$$

$$t_i = t_0 \quad \text{... (15)}$$

$$\bar{\sigma} = \sigma_y \quad \text{... (16)}$$

Where d_0 is the initial (outer) tube diameter and σ_y is the yield strength of the tube material.

Substituting Eqs. (13)–(16) into Eqs. (11) and (12) yields

$$p_{iy} = \frac{\sigma_y}{(1 - \alpha + \alpha^2)^{1/2}} \cdot \frac{2t_0}{(d_0 - t_0)} \quad \text{... (17)}$$

and

$$F_y = p_i \cdot \pi \cdot \frac{(d_0 - t_0)^2}{4} \cdot (1 - 2\alpha) \quad \text{... (18)}$$

Eqs. (17) and (18) can be used in a first attempt to determine the yield limit in tube hydroforming.

In the analysis above, F is assumed to be equal to the forming force. In other words, the sealing and friction forces are not considered in the analysis above.

Therefore, Eqs. (17) and (18) predict that the tube yields at $F = 0$ under plane stress condition,

When $\alpha = 1$ (equal biaxial stress) Eqs. (17) became is

$$p_{iy} = \sigma_y * \frac{2\,t0}{(d0 - t0)}$$

NUMERICAL SIMULATION

For simulating free bulge hydroforming process, commercial FEA software ANSYS 11 was used, in which the "Newton-Raphson" implicit approach was employed to solve nonlinear problem.

The 3-D 8-node plastic structural solid element of VISCO107 was used for work piece (blank).The tool set (die) was modeled as rigid bodies.

Automatic contact procedure in ANSYS 11 was used to model the complex interaction between the blank and tooling. For rigid (tool set)-flexible (blank) contact, 3D 8-node quadrilateral target elements of TARGE170 were used, to represent 3D target (tool set) surfaces which were associated with the deformable body (blank) represented by 3D 8-node contact elements of CONTA174. The contact and target surfaces constituted a "contact pair", which was used to represent contact and sliding between the surfaces of tool set and workpiece (blank).

free bulge hydroforming models were created. Due to the symmetry in the specimen geometry, constraints and boundary conditions, only a 1/8 portion of the tube blank had been shown in Figure (3).

The von Mises isotropic yield criterion was used in numerical simulation and their predictions compared against the experimental results of aluminum alloy (6060) tube and pure copper tube before and after heat treatment. A Coulomb friction law was employed to investigate the effect of friction at the tool-material interface. Elasto-plastic constitutive model with isotropic strain hardening was used to simulate the tube response. The elastic behavior was taken to be linear and the plastic response was modeled using the von Mises yield criterion (isotropic). Table (1) shows the mechanical properties for two materials before and after heat treatment.

Table (1) the material properties

material	Young's modulus, E (GPa)	Tangent modulus, E_t (GPa)	Yield stress, $б_y$ (MPa)	Poisson's ratio, ν	Coefficient of friction μ
Al after heat treatment	70	0.6	40	0.3	0.1
Cu after heat treatment	125	1.2	55	0.34	0.1
Al 6060	70	1.475	70	0.3	0.1
Cu	125	2.5	124	0.34	0.1

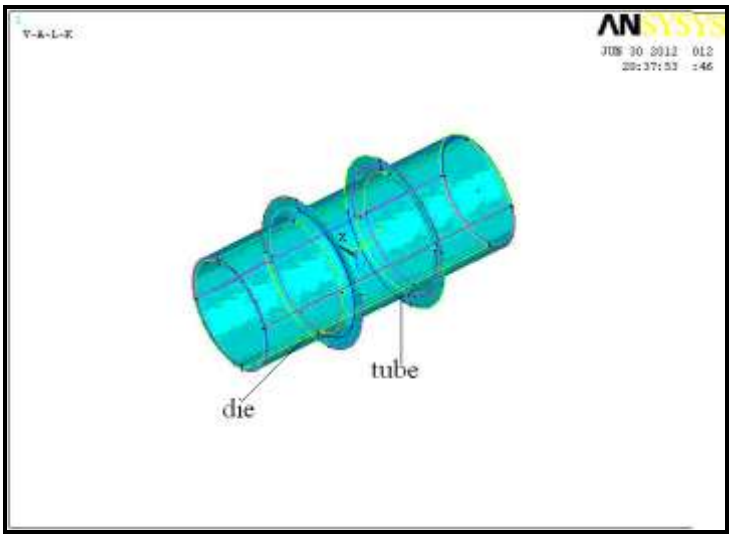

Figure (3) tube hydroforming and free bulge model.

EXPERIMENTAL WORK

In this work a free bulge die was designed and construct to carry out the experimental work shown in Figure (4).two types of hydroforming die with square cross-section for copper and aluminum alloy (6060) tubes where used. The experiments were carried out using universal testing Machine with capacity of 10 tons and cross head speed of (1mm/min) to generate hydraulic pressure by pressing hydraulic jack .

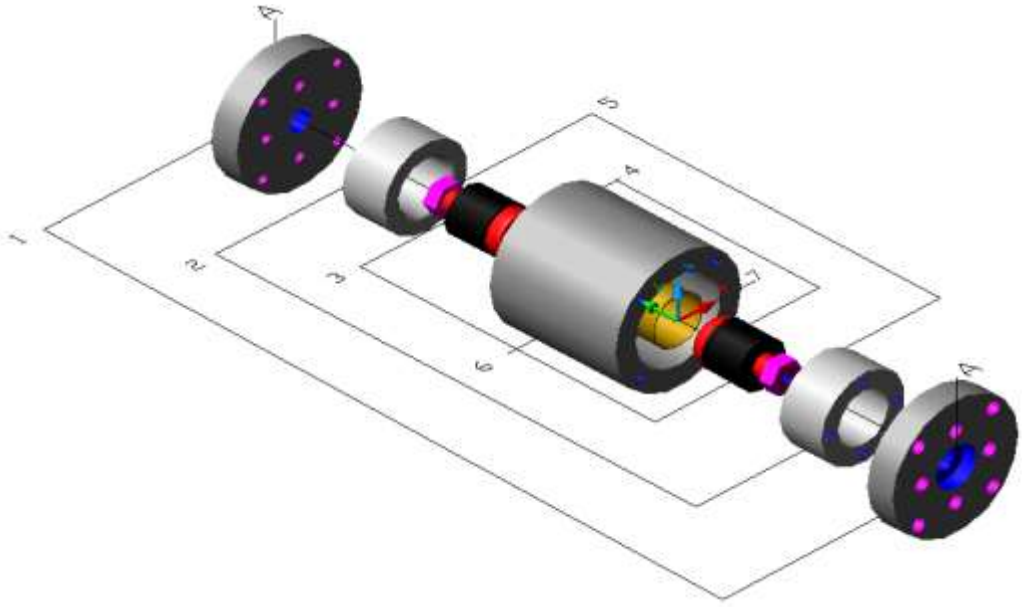

Figure (4) Isometric free bulge die.

Table (2) description parts of bulge die.

No. of part	Description	Quantity
1	Lower show and upper show (cover)	2
2	cylindrical push	2
3	urethane ring	2
4	Stud	2
5	Nut	2
6	Die	1
7	tube	1

Figure (5) free bulge die for (a) Al tube (b) Cu tube.

RESULTS AND DISCUSSION

strain measurement

The image processing technique can measure true strain of the tensile samples of copper and aluminum tubes before and after heat treatment by analysis of the grid which was printed on surface of the tensile samples in the failure region and then has been determine another variables in tables below depended on the equation (6).

Table (3) results of the tensile test of copper samples after heat treatment

Sample No	ϵ_1	ϵ_2	β
1	0.4225	-0.4544	-0.9298
2	0.41871	-0.419	-0.99931
3	0.4134	-0.4288	-0.96409

Table (4) results of the tensile test of copper samples before heat treatment

Sample No	ϵ_1	ϵ_2	β
1	0.01587	-0.07	-0.22671
2	0.01623	-0.0766	-0.21188

Table (5) results of the tensile test of al 6060 samples before heat treatment

Sample No	ϵ_1	ϵ_2	β
1	0.195566	-0.21816	-0.89643
2	0.188966	-0.208	-0.90849

Table (6) results of the tensile test of al 6060 samples after heat treatment

Sample No	ϵ_1	ϵ_2	β
1	0.2806	-0.29444	-0.953
2	0.249	-0.27444	-0.9073
3	0.2654	-0.28877	-0.91907
4	0.267	-0.27877	-0.95778

hydraulic bulge test

As already said the experimental campaign was carried out on copper and aluminum tubes before and after heat treatment. The experiments were conducted at different pressure levels in order to obtain the relationship between bulge height, thickness and pressure. A square grid was etched on each tube to measure the hoop and the longitudinal strain at the end of the process so to verify the deformations calculated by the analytical model. Figures (6) and (7) show the copper and aluminum tubes at the end of the process experimentally and numerically. The bulge area is plastically deformed. During the test the axial actuators are still and the tube is fully blocked. The experiments design starts from the observation of the tube bursting pressure and yield pressure. Within this range other different pressure levels have been investigated. For each tested tube the bulge height, the radius of curvature in the longitudinal direction and the wall thickness were measured. From these experimental values. The results show in the tables below.

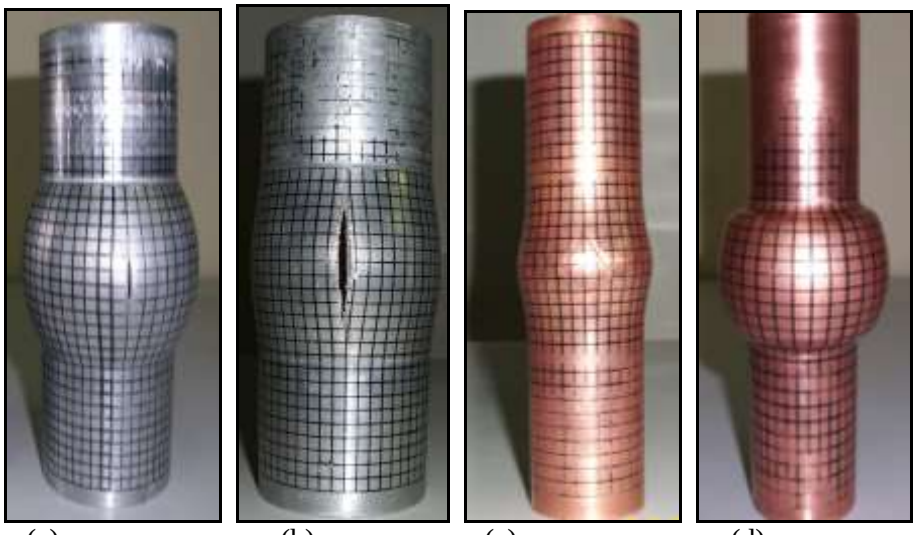

(a) (b) (c) (d)

Figure (6) experimental final tubes at bursting a- Al 6060 tube after heat treatment b- Al 6060 tube without heat treatment c- cu tube without heat treatment d- cu tube after heat treatment.

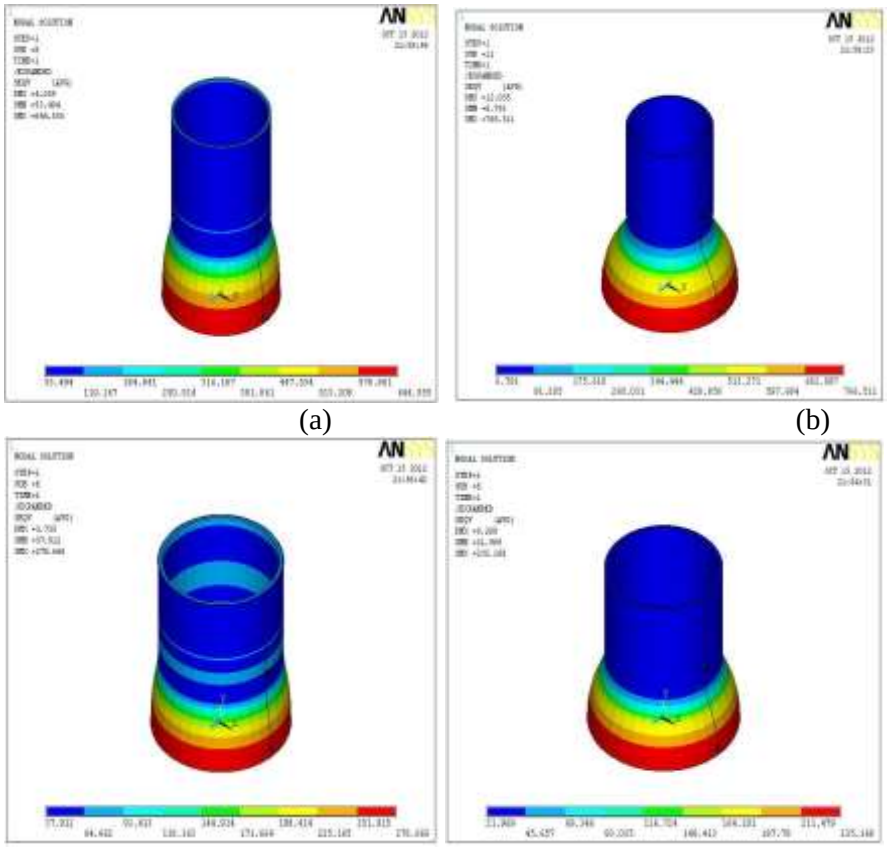

(a) (b)

(c) (d)

Figure (7) numerical Von-Mises stress of final tubes at bursting a- cu tube without heat treatment b- Cu tube after heat treatment c- Al 6060 tube without heat treatment d- Al 6060 tube after heat treatment.

Stress and strain distribution

Figures (7), (8) show the distribution of Von-Mises stress and strain in the final formed copper and aluminum tubes before and after heat treatment in the hydraulic bulge test. It can be seen from the Figure (7), (8) that the maximum Von-Mises stress and strain are located in the pole of the tube.

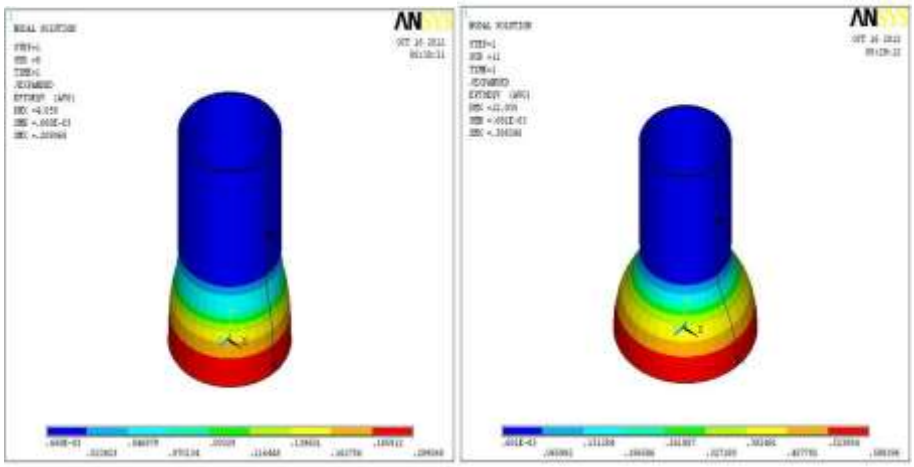

a b

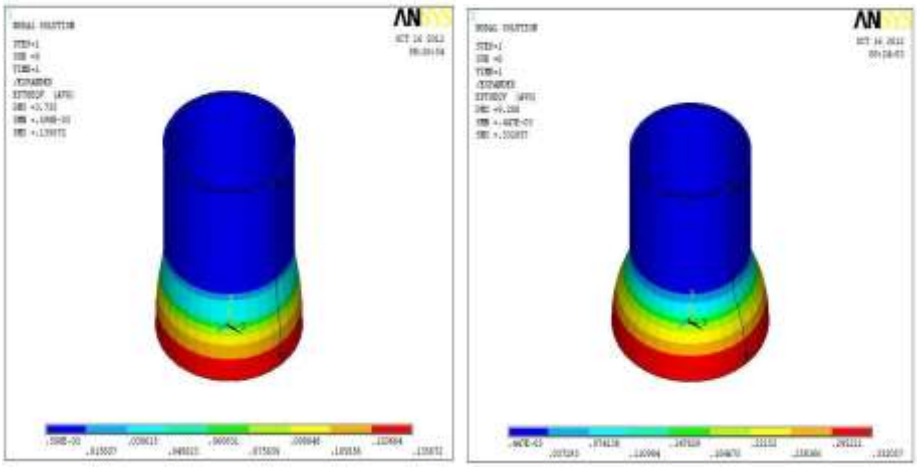

c d

Figure (8) numerical Von-Mises strain of final tubes at bursting a- cu tube without heat treatment b- Cu tube after heat treatment c- Al 6060 tube without heat treatment d- Al 6060 tube after heat treatment.

Table (7) experimental and numerical results of bulge test for aluminum tube after heat treatment

level	Pressure (MPa)	Numerical result			Experimental result	
		Outer radius (mm)	bulge height(mm)	Thickness (mm)	Outer radius(mm)	bulge height(mm)
1	0	30	0	2	30	0
2	2	30.1195	0.1195	1.9997	30.01	0.01
3	4	30.23707	0.23707	1.987	30.215	0.215
4	6	31.767	1.767	1.8966	31.655	1.655
5	8	33.343	3.343	1.8079	33.258	3.258
6	10	34.942	4.942	1.7198	34.89	4.89
7	12	36.367	6.367	1.6431	36.255	6.255
8	14	37.772	7.772	1.5657	37.67	7.67
9	16	39.208	9.208	1.4871	39.178	9.178

Table (8) experimental and numerical results of bulge test for aluminum tube before heat treatment.

level	pressure (MPa)	Numerical result			Experimental result	
		Outer radius (mm)	bulge height(mm)	Thickness (mm)	Outer radius (mm)	bulge height(mm)
1	0	30	0	2	30	0
2	2	30.012	0.011951	1.9997	30	0
3	4	30.0239	0.023889	1.9994	30.03	0.03
4	6	30.0512	0.051233	1.9983	30.045	0.045
5	8	30.4614	0.461429	1.974	30.449	0.449
6	10	31.05	1.05	1.94	31	1
7	12	31.641	1.641	1.907	31.577	1.577
8	14	32.241	2.241	1.8737	32.185	2.185
9	16	32.854	2.854	1.84	32.778	2.778
10	18	33.472	3.472	1.8061	33.335	3.335
11	19	33.784	3.784	1.7919	33.699	3.699

Table (9) experimental and numerical results of bulge test for Copper tube after heat treatment.

level	pressure (MPa)	Numerical result			Experimental result	
		Outer radius (mm)	bulge height(mm)	Thickness (mm)	Outer radius(mm)	bulge height(mm)
1	0	20.64	0	1.06	20.64	0
2	2	20.70015	0.06015	1.059	20.64	0
3	4	20.8447	0.2047	1.05	20.78	0.14
4	6	21.488599	0.848599	1.0215	21.305	0.665
5	8	22.186	1.546	0.9914	22.06	1.42
6	10	22.966	2.326	0.9588	23.37	2.73
7	12	23.847	3.207	0.9236	23.76	3.12
8	14	24.826	4.186	0.8859	24.69	4.05
9	16	25.884	5.244	0.8468	25.76	5.12
10	18	26.889	6.249	0.8122	26.792	6.152
11	20	28.007	7.367	0.7717	27.92	7.28
12	22	29.215	8.575	0.7298	29.135	8.495
13	24	30.485	9.845	0.688	30.373	9.733
14	26	31.93	11.29	0.643	31.863	11.223
15	27	32.675	12.035	0.621	32.642	12.002

Table (10) experimental and numerical results of bulge test for Copper tube before heat treatment.

level	pressure (MPa)	Numerical result			Experimental result	
		Outer radius(mm)	bulge height(mm)	Thickness (mm)	Outer radius(mm)	bulge height(mm)
1	0	20.64	0	1.06	20.64	0
2	2	20.646	0.006015	1.0599	20.64	0
3	4	20.652	0.012024	1.0598	20.64	0
4	6	20.658	0.01802	1.0596	20.652	0.012
5	8	20.7429	0.102857	1.056	20.74	0.1
6	10	21.031	0.390986	1.043	21.0275	0.3875
7	12	21.339	0.698959	1.0288	21.323	0.683
8	14	21.657	1.017	1.015	21.648	1.008
9	16	21.994	1.354	1.0002	21.962	1.322
10	18	22.351	1.711	0.9852	22.329	1.689
11	20	22.726	2.086	0.9694	22.713	2.073
12	22	23.122	2.482	0.953	23.029	2.389
13	24	23.541	2.901	0.9363	23.52	2.88
14	26	23.985	3.345	0.919	23.937	3.297
15	28	24.451	3.811	0.9011	24.419	3.779
16	29	24.699	4.059	0.8918	24.648	4.008

Table (11) numerical and experimental result of the final stage al 6060 tube after heat treatment in a bulge region only

pressure	Grid mm	Numerical result				Experimental result			
		ϵ_1	ϵ_2	ϵ_3	Thickness (mm)	ϵ_1	ϵ_2	ϵ_3	Thickness (mm)
16 MPa	30	0.0999	0.0266	-0.1265	1.92635	0.072	0.026	-0.098	1.813298
	25	0.133	0.0364	-0.1694	1.77244	0.089	0.04433	-0.133	1.750352
	20	0.166	0.0461	-0.2121	1.63342	0.16	0.05448	-0.2144	1.613909
	15	0.199	0.056	-0.255	1.58388	0.247	0.0595	-0.3065	1.472037
	10	0.233	0.066	-0.299	1.5204	0.26	0.06454	-0.3245	1.445719
	5	0.266	0.0755	-0.3415	1.50182	0.25	0.08	-0.33	1.437847
	0	0.2999	0.0852	-0.3851	1.4871	0.3	0.09	-0.39	1.35411

Table (12) numerical and experimental result of the final stage al 6060 tube in a bulge region only.

pressure	gridmm	Numerical result				Experimental result			
		ϵ_1	ϵ_2	ϵ_3	Thickness (mm)	ϵ_1	ϵ_2	ϵ_3	Thickness (mm)
19 MPa	30	0.04145	0.0024	-0.04385	1.9332	0.0315	0.008	-0.0395	1.92254
	25	0.05514	0.007	-0.06215	1.93158	0.055	0.009	-0.064	1.87600
	20	0.06884	0.0114	-0.08024	1.859025	0.07	0.0132	-0.0832	1.84033
	15	0.08254	0.0159	-0.09844	1.831788	0.09	0.017	-0.107	1.79705
	10	0.09623	0.02	-0.11623	1.80501	0.1	0.02	-0.12	1.77384
	5	0.11	0.025	-0.135	1.79709	0.115	0.0263	-0.1413	1.73645
	0	0.124	0.03	-0.154	1.7919	0.125	0.032	-0.157	1.7094

Table (13) numerical and experimental result of the final stage cu tube after heat treatment in a bulge region only.

pressure	gridmm	Numerical result				Experimental result			
		ϵ_1	ϵ_2	ϵ_3	Thickness (mm)	ϵ_1	ϵ_2	ϵ_3	Thickness (mm)
27 MPa	30	0.1565	0.04	-0.1965	0.98966	0.15	0.04	-0.19	0.876576
	25	0.2086	0.0561	-0.2647	0.82386	0.21	0.0567	-0.266	0.811784
	20	0.2607	0.0716	-0.3323	0.74889	0.29	0.073	-0.363	0.73732
	15	0.313	0.0871	-0.4001	0.71424	0.32	0.0878	-0.4078	0.70501
	10	0.365	0.1025	-0.4675	0.66322	0.386	0.103	-0.489	0.650034
	5	0.417	0.1180	-0.5350	0.64164	0.43	0.121	-0.551	0.610956
	0	0.469	0.133	-0.602	0.621	0.48	0.1377	-0.617	0.571534

Table (14) numerical and experimental result of the final stage cu tube in a bulge region only.

pressure	gridmm	umerical result				Experimental result			
		ϵ_1	ϵ_2	ϵ_3	Thickness (mm)	ϵ_1	ϵ_2	ϵ_3	Thickness (mm)
29 MPa	30	0.0625	0.007	-0.0695	1.029779	0.046	0.011	-0.057	1.00127
	25	0.0832	0.0118	-0.095	0.990378	0.062	0.0165	-0.078	0.98007
	20	0.104	0.0166	-0.1206	0.936702	0.11	0.022	-0.132	0.928921
	15	0.125	0.0215	-0.1465	0.917229	0.12	0.027	-0.147	0.91509
	10	0.145	0.0263	-0.1713	0.899505	0.14	0.0285	-0.1685	0.89562
	5	0.166	0.0311	-0.1971	0.895355	0.156	0.0352	-0.191	0.875525
	0	0.1866	0.036	-0.2226	0.8918	0.179	0.0375	-0.216	0.853652

Figures (9), (10), (11) and (12) show relationship between internal pressure and bulge height in the bulge test of copper and aluminum tubes before and after heat treatment , in tube hydroforming in square die must be not increase the bursting pressure value of bulge test as show in the Tables (7) to (10).

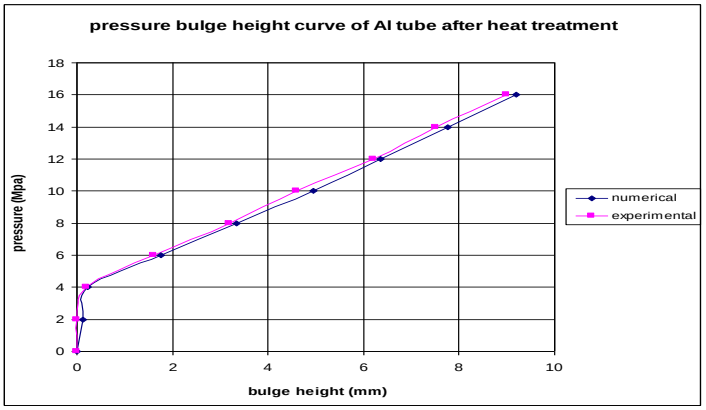

Figures (9) relationship between internal pressure and bulge height of aluminum tube after heat treatment.

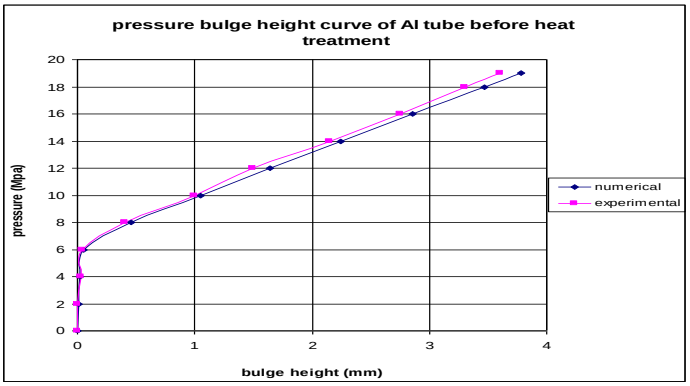

Figures (10) relationship between internal pressure and bulge height of aluminum tube before after heat treatment.

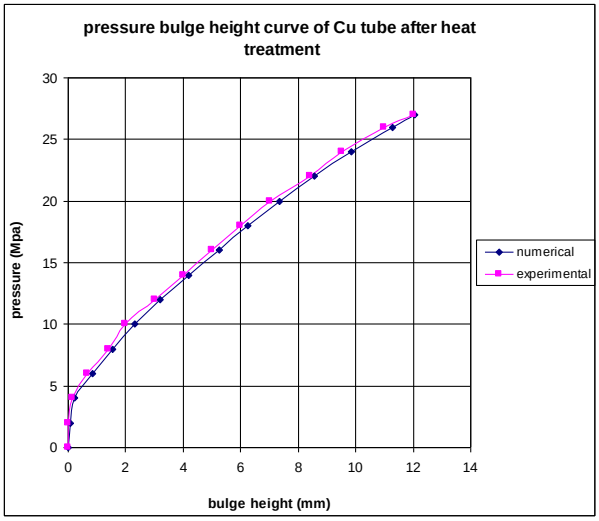

Figures (11) relationship between internal pressure and bulge height of copper tube after heat treatment

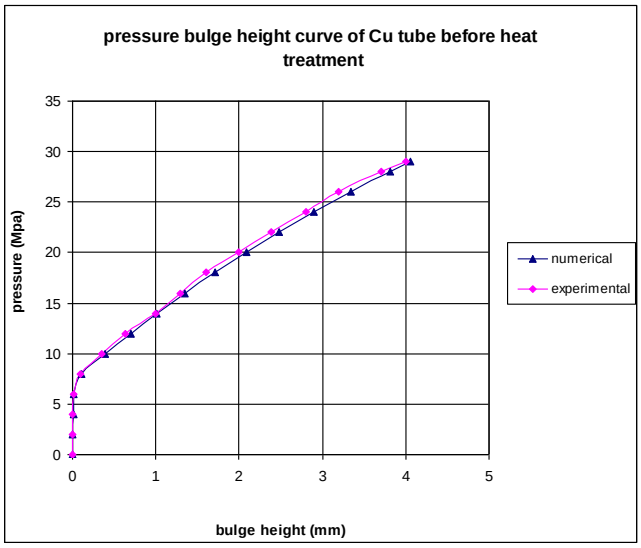

Figures (12) relationship between internal pressure and bulge height of copper tube before after heat treatment

Thickness distribution

Figure (13) shows thickness distributions and location of thinning in the bulge test of copper and aluminum tubes before and after heat treatment. The minimum simulated thickness of tube Aluminum tubes before and after heat treatment (1.7919, 1.4871) mm .While it is reduced from 2 mm to (1.7094, 1.35411) mm by experimental test at pressures (19, 16) MPa. The variation between simulated and experimental tests results are (4.8, 9.8) %, and the minimum simulated thickness of tube copper tubes before and after heat treatment (0.8918, 0.621) mm .While it is reduced from 1.06 mm to (0.853652, 0.571534) mm by experimental test at pressures (29, 27) MPa. The variation between simulated and experimental tests results are (4.4, 8.6) %.

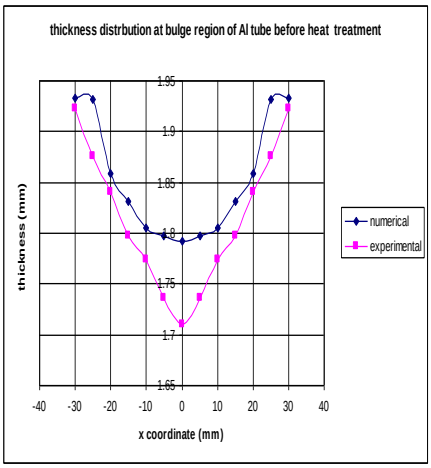

a

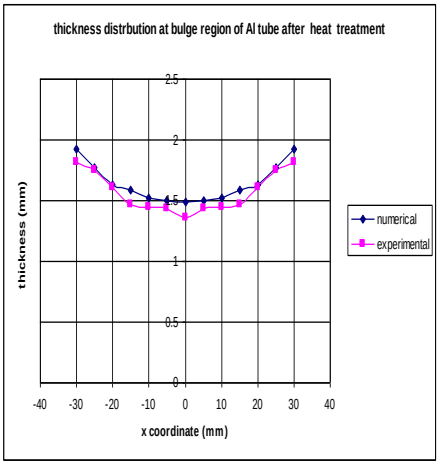

b

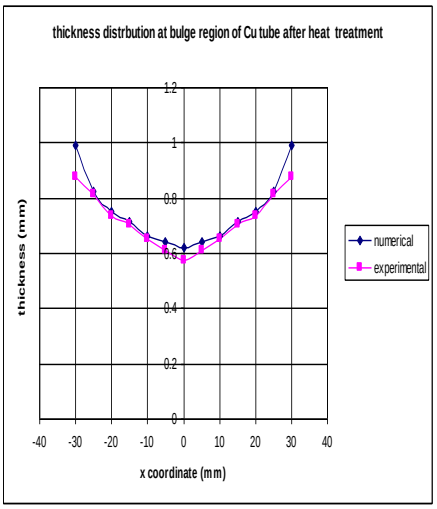

d

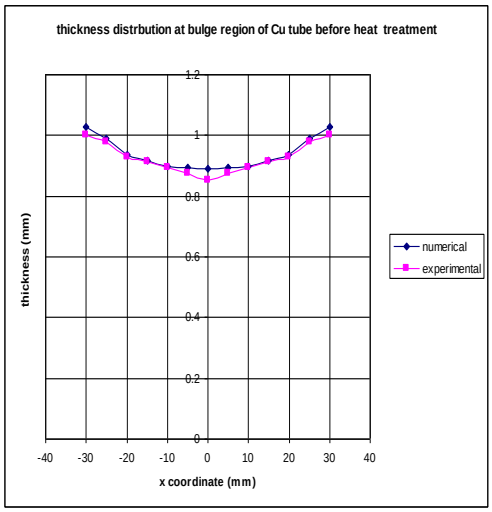

c

Figure (13)show the tube thickness along its bulged part at the end test a- Al 6060 tube without heat treatment b- Al 6060 tube after heat treatment c- Cu tube after heat treatment d- cu tube without heat treatment.

Determine hydraulic yield pressure

From Equation (2-17) and depended on mechanical properties and dimensions of the copper and aluminum tubes before and after heat treatment can determine yield pressure in the bulge test and determine yield pressure numerically and experimentally from the Tables (7) to (10) , the results show in the table below.

Table (15) show values yield pressure in the bulge test

Tube materials	Yield pressure (Mpa)		
	Experimentally	numerically	theoretically
Al before heat treatment	4	4	4.83
Al after heat treatment	2	2	2.75
Cu before heat treatment	6	4	6.537
Cu after heat treatment	4	2	2.89

forming limit diagram

To find forming limit diagram of copper and aluminum tubes before and after heat treatment depended on tensile test and bulge test and strain hardening exponent (n) by drawing strain paths data , and show in Figure (14).

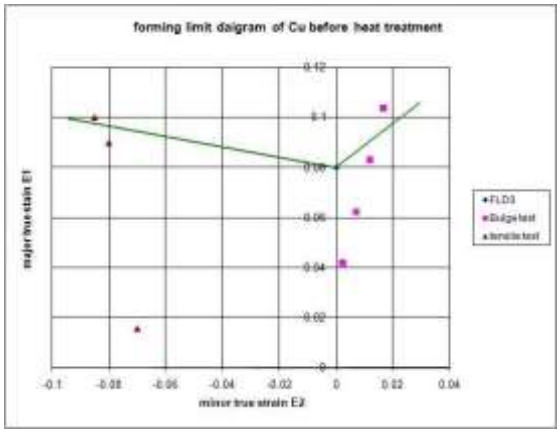

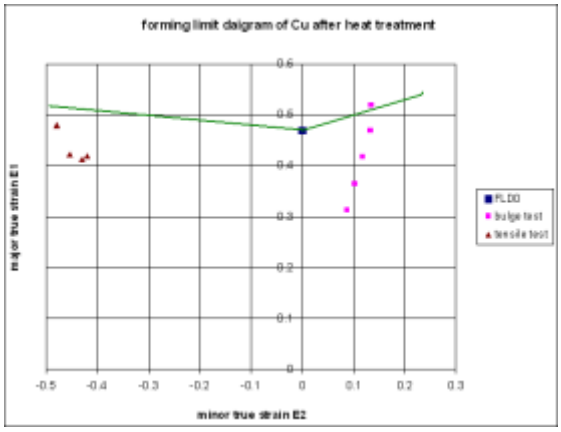

a

b

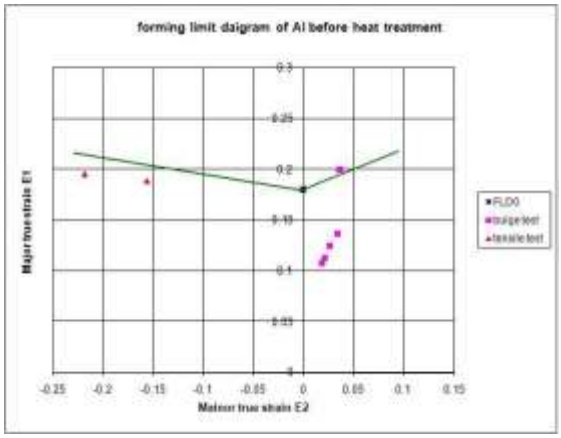

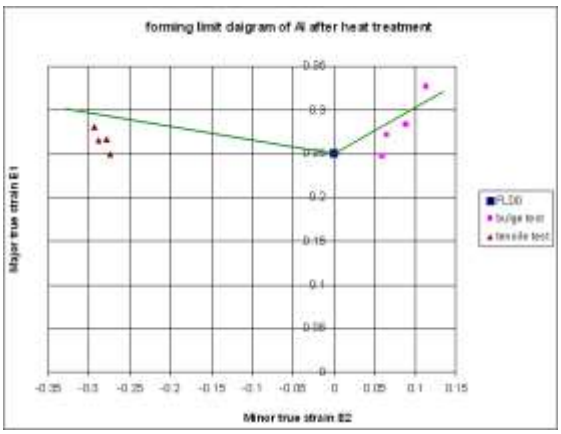

c

d

Figures (14) forming limit diagram of a- cu tube without heat treatment b- Cu tube after heat treatment c- Al 6060 tube without heat treatment d- Al 6060 tube after heat treatment

From the figure above it can be noted that aluminum and copper tubes after heat treatment good formability comparison with aluminum and copper tubes before heat treatment.

REFERENCES

[1].Ahmed, M., Hashmi, M.S.J., 1997. Estimation of machine parameters for hydraulic bulge forming of tubular components. J. Mater. Proc. Technol. 64, 9–23.

[2].Ahmetoglu, M., Sutter, K., Li, X.J., Altan, T., 2000. Tube hydroforming: current research, applications and need for training. J. Mater. Proc. Technol. 98, 224–231.

[3].Asnafi, N., Skogsgardh, A., 2000. Theoretical and experimental analysis of stroke controlled tube hydroforming. J. Mater. Sci. Eng. A 279, 95–110.

[4].Chen,W.F.,Han,D.J., 1995. Plasticity for Structural Enginners.GauLihBookCo., Taipei, Taiwan, pp. 181–189.

[5].Dohmann, F.,Hartl, Ch., 1996.Hydroforming a method to manufacture light-weight parts. J. Mater. Proc. Technol. 60, 669–676.

[6].Hill, R., 1952. On discontinuous plastic states, with special reference of localized necking in thin sheets. J. Mech. Phys. Solids 1, 19–30.
[7].Hill, R., 1979. Theoretical plasticity of textured aggregates. Mathematical Proceedings of the Cambridge Philosophical Society, p. 17.
[8].Hwang, Y.M., Huang, L.S., 2005. Friction tests in tube hydroforming. Proc. Inst.Mech Eng. B: J. Eng. Manufact. 219, 587–594.
[9].Hwang, Y.M., Lin, Y.K., 2006. Analysis of tube bulge forming in an open die consider ing anisotropic effects of the tubular material. Int. J. Mach. Tools Manufact. 46, 1921–1928.
[10].Hwang, Y.M., Lin, Y.K., 2007. Evaluation of flow stresses of tubular materials con sidering anisotropic effects by hydraulic bulge tests. Tran. ASME, J. Eng. Mater. Technol. 129, 414–421.
[11].Hwang, Y.M., Lin, Y.K., Altan, T., 2007a. Evaluation of tubularmaterials by a hydraulic bulge test. Int. J. Mach. Tools Manufact. 47, 343–351.
[12].Hwang, Y.M., Lin, T.C., Chang, W.C., 2007b. Experiments on T-shape hydroforming with counter punch. J. Mater. Proc. Technol. 192–193, 243–248.
[13].Korkolis, Y.P., Kyriakides, S., 2008. Inflation and burst of anisotropic aluminum tubes for hydroforming applications. Int. J. Plasticity 24, 509–543.
[14].Koc, M., Aue-u-lan, Y., Altan, T., 2001. On the characteristics of tubular materials for hydroforming—experimentation and analysis. Int. J. Mach. Tools Manufact. 41, 761–772.
[15].Lei, L.P., Kim, J., Kang, B.S., 2002. Bursting failure prediction in tube hydroforming processes by using rigid–plastic FEM combined with ductile fracture criterion. Int. J. Mech. Sci. 44, 1411–1428.
[16].Nefussi, G., Combescure, A., 2002. Coupled buckling and plastic instability for tube hydroforming. Int. J. Mech. Sci. 44, 899–914.
[17].Sokolowski, T., Gerke, K., Ahmetoglu,M., Altan, T., 2000. Evaluation of tube formability and material characteristics: hydraulic bulge testing of tubes. J. Mater. Proc. Technol. 98, 34–40.
[18].Strano, M., Altan, T., 2004. An inverse energy approach to determine the flow stress of tubular materials for hydroforming applications. J. Mater. Proc. Technol. 146, 92–96.
[19].Swift, H.W., 1952. Plastic instability under plane stress. J. Mech. Phys. Solids 1, 1–18.
[20].Tirosh, J., Neuberger, A., Shirizly, A., 1996. On tube expansion by internal fluid pressure with additional compressive stress. Int. J. Mech. Sci. 38, 839–851.
[21].Vollertsen, F., Plancak, M., 2002. On possibilities for the determination of the coefficient of friction in hydroforming of tubes. J. Mater. Proc. Technol. 125-126, 412–420.
[22].Xing, H.L., Makinouchi, A., 2001. Numerical analysis and design for tubular hydroforming. Int. J. Mech. Sci. 43, 1009–1026.
[23].Yoshida, K., Kuwabara, T., 2007. Forming limits of aluminum alloy tubes under axial load and internal pressure. Int. J. Plasticity 23, 1260–1284.
[24].Zhao, L., Sowerby, R., Sklad,M.P., 1996. A theoretical and experimental investigation of limit strains in sheet metal forming. Int. J. Mech. Sci. 38, 1307–1317 .